表1　松果体腫瘍の組織学的分類

神経上皮性腫瘍	松果体部腫瘍	松果体細胞腫
		中間型松果体実質細胞腫
		松果体芽腫
		松果体部乳頭状腫瘍
胚細胞腫	ジャーミノーマ	
	胎児性癌	
	卵黄嚢腫瘍	
	絨毛癌	
	奇形腫	成熟奇形腫
		未熟奇形腫
		悪性転化を伴う奇形腫
	混合胚細胞系腫瘍	

日本脳神経外科学会，日本病理学会，脳腫瘍取扱い規約 第3版，金原出版，東京，2010．[3]

表2　胚細胞腫の臨床的分類

予後良好群	成熟奇形腫
	ジャーミノーマ
予後中間群	未熟奇形腫
または中等度悪性群	悪性転化を伴う奇形腫
	ジャーミノーマあるいは未熟奇形腫を主体とする混合腫瘍
予後不良群	胎児性癌
または高度悪性群	卵黄嚢腫瘍
	絨毛癌
	上記3組織型を主体とする混合腫瘍

ない．また何よりも，腫瘍，特に全摘出が治癒への必要条件とも考えられる予後中間群や予後不良群の胚細胞腫では，早晩直達手術が必要になる可能性が残る．

考え方としては，[illegible]による水頭症を合併している場合，[illegible]開窓術を主目的とし，ついでに腫瘍をデブというスタンスで神経内視鏡手術を行う．[illegible]にジャーミノーマが示唆された場合などは，このような腫瘍摘出を主目的とした直達手術を行うことを考えるべきであろう．

ただし直達手術は，放射線・化学療法後に行うというオプションもある．腫瘍が大きく患者の意識状態が悪く，直達手術による大きな侵襲が危惧される場合などは，化学療法あるいは放射線療法を先行させて腫瘍の縮小を図り，必要に応じて直達手術を後から行うといった柔軟な姿勢が必要になる場合もある．

Occipital transtentorial approach

わが国においては，infratentorial supracerebellar approach は主流ではない．座位を取らなければならないことが最大の欠点と考えられる[1]．本稿では，occipital transtentorial approach について概要を述べる．

体位は腹臥位であるが，まず患者の右肩越しにアプローチするか左肩越しにアプローチするかを決めなければならない．血管撮影あるいは MR venography（MRV）によって皮質静脈の分布を観察し，これが妨げにならない側からのアプローチを選択する．

脳室ドレナージは必須である．開頭の皮切は図1のようになる．Transverse sinus あるいは conflu-

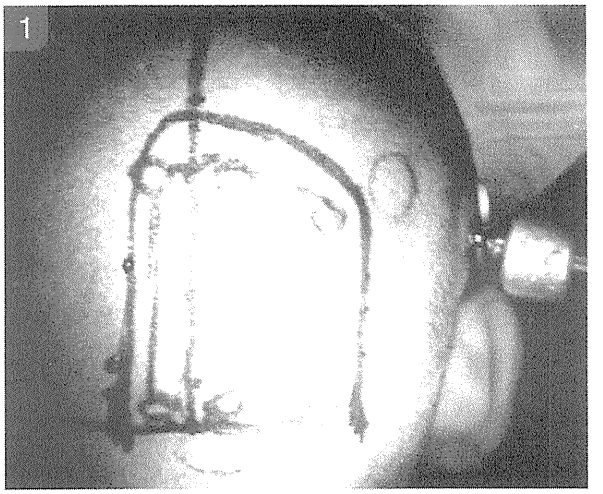

図1　右 OTA における皮切と開頭デザイン（症例1）

GO → WEB

ence を露出する必要があるため，その高位をきちんと確認することが大事である．これは navigation を用いていれば容易に確認できる．

小脳天幕の切開は直静脈洞に近づきすぎないように注意する（図 2）．後頭葉を横方向に引きがちであるが，注意しないと前方へ行きすぎてしまうきらいがある．大脳鎌と小脳天幕の移行部に脳べらを入れて，少しずつ大脳鎌の方向にずらしていきながら後頭葉を持ち上げていく感覚で進めると，直静脈洞からテント自由縁が確認される．

テント自由縁において厚いくも膜を切開し，Galen 大静脈の位置を確認し，左右に最大限切開を広げると腫瘍が出現する（図 3）．腫瘍は表面のくも膜を可能な限り広く剥離した後に piece by piece に摘出する．腫瘍が前方に大きく張り出している場合には，posterior transcallosal approach を併用する（図 4A）．

最後に第三脳室を確認する（図 4B，5）．中脳四丘体からの剥離は特に慎重にしないと，術後の眼球運動障害が重篤になる．術中写真を供覧した

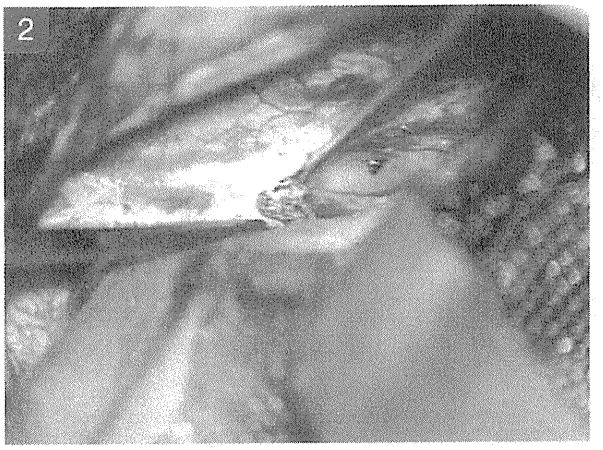

図 2　右 OTA における小脳テント切開（症例 1）
直静脈洞から離れた方向に切り上げてくる．

図 3　くも膜切開（症例 1）
小脳テント自由縁において分厚いくも膜を切開したところ．直下に赤灰色の腫瘍が観察されている．

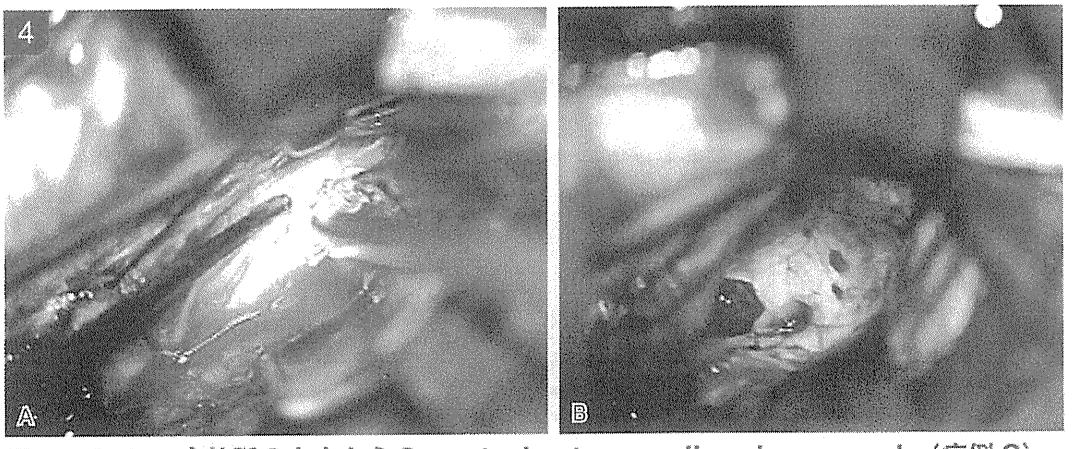

図 4　Galen 大静脈の上方からの posterior transcallocal approach（症例 2）
A：脳梁膨大部の切開．B：摘出後に第三脳室をのぞき込んだところ．

症例のMRIを示す（図6，7）．

予後中間群や予後不良群では，化学療法や放射線療法を先行させてから摘出術を行うオプションがあることは前述したが，症例を呈示する．

症　例（症例3）

14歳，男児．頭痛，嘔吐で発症し松果体部腫瘤と水頭症が認められた．血清AFP＝22,398であった．前医にてV-P shuntを行った後にCBDCA＋etoposideによる化学療法が1コース行われた時点で紹介となった．当院では，全脳脊髄30 Gy＋腫瘍局所30 Gyの放射線療法を行った．図8に初発時と放射線療法終了時のMRIを示すが，腫瘍縮小効果に乏しいため，摘出手術となった．腫瘍は表面が平滑でつるっとした腫瘤で，摘出は容易であった（図9）．腫瘤内部には，類上皮腫を思わせるもろもろとした部分や一部には毛髪も認められた．組織は未熟奇形腫であった．初発時は卵黄嚢腫瘍であったものが，化学療法と放射線療法によって奇形腫に変化したものと考えられる．

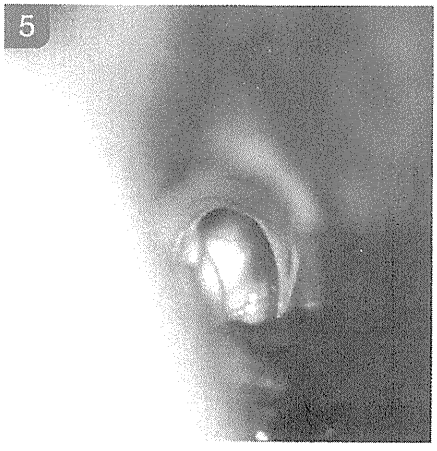

図5　腫瘍摘出後（症例1）
腫瘍摘出後に第三脳室をのぞき込んでいるところ．

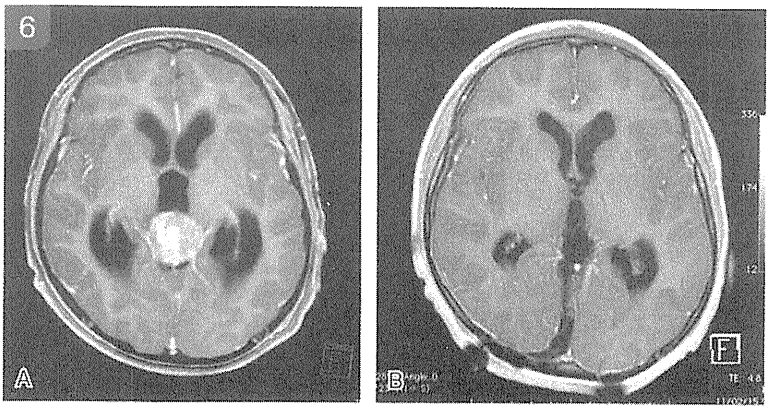

図6　症例1の造影MRI
術前（A）と術後（B）．組織は胎児性癌であった．

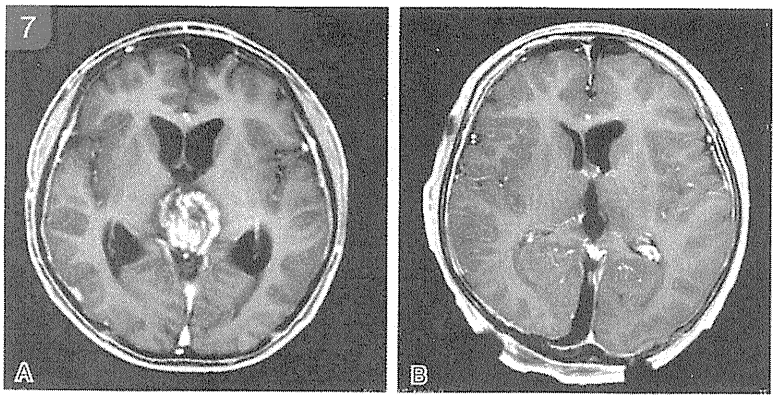

図7　症例2の造影MRI
術前（A）と術後（B）．組織は未熟奇形腫であった．

GO → WEB

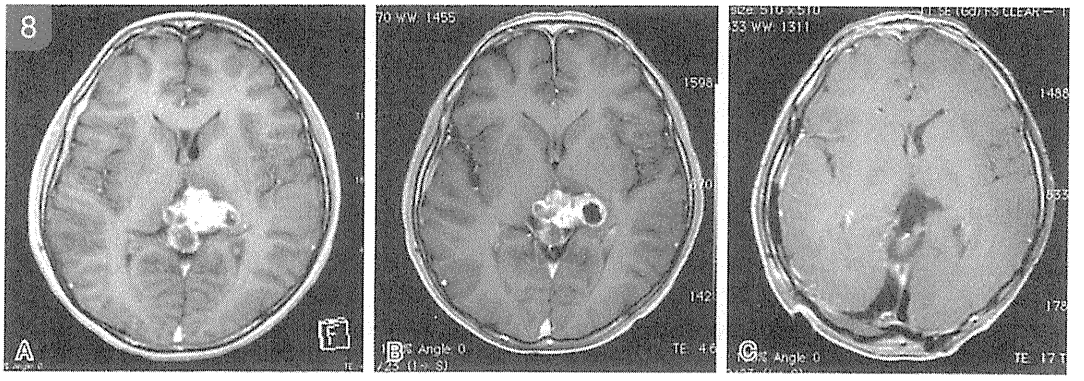

図 8　症例 3 の造影 MRI
初発時（A），化学療法と放射線療法後（B）と術後（C）．

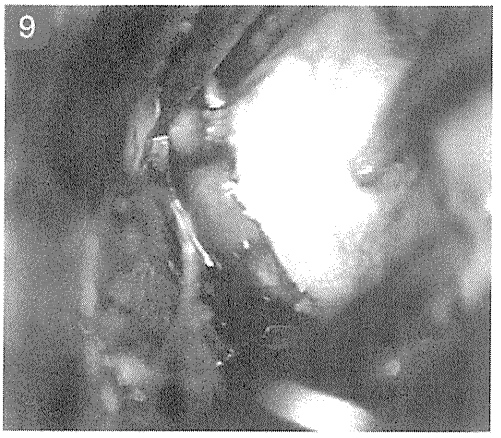

図 9　術中所見（症例 3）
腫瘍は表面平滑で摘出は容易であった．

放射線・化学療法の組み立て

2010 年暮れからオープン参加の臨床試験が開始されている．従来，厚生労働省研究班という限られた施設で行われていた．しかし世界に誇るべき治療方針を，広くどの施設でも行えるようにすることを目的の一つとしてオープン化された．以下に概要を述べる．

臨床試験名

初発の頭蓋内原発胚細胞腫に対する放射線・化学療法第 II 相臨床試験

試験デザイン

中央登録方式による多施設自由（オープン）参加臨床第 II 相試験

患者選択基準（抜粋，要約）

1 成熟奇形腫を除く頭蓋内原発胚細胞腫初発症例．

2 組織学的に診断が得られているか，あるいは組織診断は得られていないが血清 HCG 値が 2,000 mIU/mL 以上あるいは血清 AFP 値が 2,000 ng/mL 以上．

3 4 歳以上．

4 PS が 0 ～ 2 の症例．ただし，腫瘍による神経症状のみに起因する PS 3 は許容．

5 化学療法に耐えられる検査値基準を満たす．

6 術後 4 週間以内に一次治療を開始できること．

7 文書による同意が得られていること．

除外基準（抜粋，要約）

1 脳腫瘍以外の悪性腫瘍の既往がある症例．

2 化学療法の妨げとなる腎，膀胱，感染症，肺，心臓，肝臓，精神障害，糖尿病，過敏症などの疾患や障害を有する症例．

3 妊娠中，授乳中あるいは妊娠の可能性がある女性．

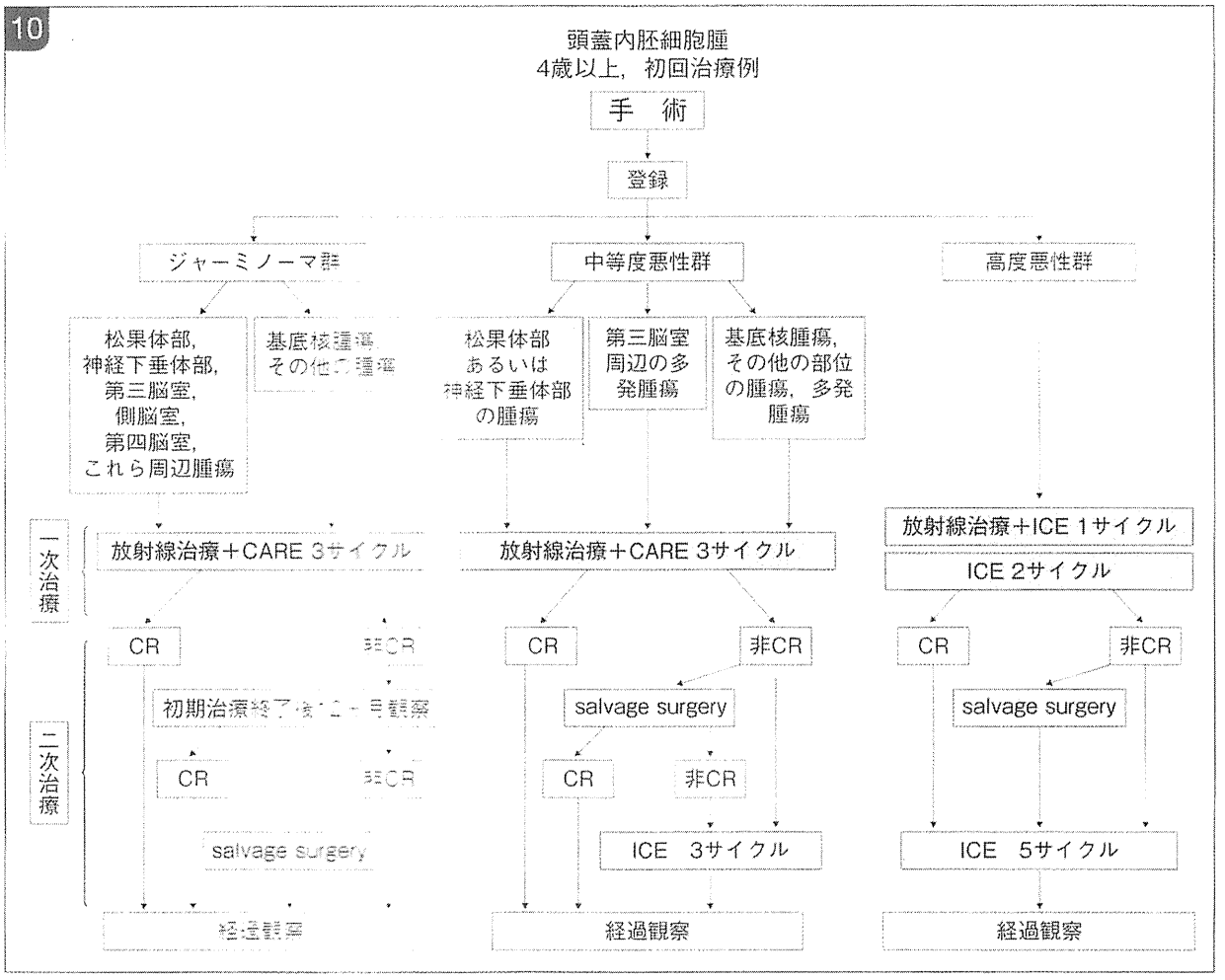

図 10　胚細胞腫瘍臨床試験のシェーマ

治療方法

1　ジャーミノーマ

①放射線療法と化学療法を同時にスタートする．

②放射線療法は全脳室照射を原則として 1.8 Gy × 13 fr = 23.4 Gy を照射する．

③基底核腫瘍の場合は全脳照射とする．

④化学療法は以下のレジメンを 28 日を 1 サイクルとして 3 回行う．

Day 1: carboplatin 450 mg/m^2

Day 1 ～ 3: etoposide 150 mg/m^2

⑤以上の一次治療終了後は経過観察とする．1 年後においても腫瘍陰影が残存する場合は，必要に応じて再手術を行う．

2）中等度悪性群

①放射線療法と化学療法を同時にスタートする．

②放射線療法は全脳室照射 23.4 Gy ＋腫瘍局所照射 27.0 Gy を原則とする．

③基底核，脳内多発腫瘍などでは全脳照射を行う．

④化学療法は carboplatin+etoposide を 28 日を 1 サイクルとして 3 回行う．

JJCO Japanese Journal of Clinical Oncology

Jpn J Clin Oncol 2010;40(8)788–794
doi:10.1093/jjco/hyq044
Advance Access Publication 20 April 2010

Clinical Outcomes of Stereotactic Brain and/or Body Radiotherapy for Patients with Oligometastatic Lesions

Tetsuya Inoue[1,*], Norio Katoh[1], Hidefumi Aoyama[1], Rikiya Onimaru[1], Hiroshi Taguchi[1], Shunsuke Onodera[1], Satoshi Yamaguchi[2] and Hiroki Shirato[1]

[1]Department of Radiology, Hokkaido University Graduate School of Medicine and [2]Department of Medical Physics, Hokkaido University Graduate School of Medicine, Sapporo, Japan

*For reprints and all correspondence: Tetsuya Inoue, Department of Radiology, Hokkaido University Graduate School of Medicine, North 15 West 7, Kita-ku, Sapporo 060-8638, Japan. E-mail: t-inoue@med.hokudai.ac.jp

Received November 30, 2009; accepted March 11, 2010

Objective: Several recent studies have shown that oligometastatic disease has curative potential, although it was previously considered to signal a patient's last stage of life. Stereotactic body radiotherapy has been available for extra-cranial metastases in addition to stereotactic cranial radiotherapy for brain metastases. The aim of the present study was to retrospectively evaluate the clinical outcomes of stereotactic radiotherapy for patients with oligometastatic lesions.

Methods: Between 1999 and 2008, 41 patients with five or fewer detectable metastases were treated with stereotactic radiotherapy at our institution. The treated oligometastatic lesions were in the brain, lung and adrenal glands.

Results: With a median follow-up period of 20 months, the 3-year overall survival, progression-free survival, local control and distant control rates were 39%, 20%, 80% and 35%, respectively, and the respective 5-year rates were 28%, 20%, 80% and 35%. The median survival time was 24 months. According to interval to recurrence, the 3- and 5-year overall survival rates were 19% and 10%, respectively, for patients with <12 months ($n = 18$), compared with 53% and 40% for those with ≥ 12 months ($n = 23$) ($P = 0.006$).

Conclusions: Precise stereotactic radiotherapy was effective in controlling oligometastatic lesions for patients with a median survival time of 24 months. Interval to recurrence may impact the overall survival rate and should be included in the stratification criteria in a prospective randomized trial to investigate the benefits of stereotactic radiotherapy for patients with oligometastases.

Key words: oligometastases – stereotactic body radiotherapy – stereotactic radiotherapy – radiosurgery

INTRODUCTION

Most patients who have had any recurrent or metastatic sites of cancer are considered to be in their last stage of life. However, stereotactic cranial radiosurgery (SCRS) and stereotactic cranial radiotherapy (SCRT) have been shown to be useful for prolonging useful life in patients with solitary or oligo brain metastases with or without whole brain radiotherapy (WBRT) (1,2). The treatment outcomes are related to the number of metastases and the presence or absence of extra-cranial disease (3). A Phase III study has suggested that SCRS with WBRT results in better survival than WBRT alone for patients with a single brain metastasis or patients with tumors > 2.0 cm in diameter (4). These studies have shed light on the possibility of improving treatment outcomes by using high-dose local radiotherapy with or without whole-body cancer treatment in patients with extra-cranial metastasis.

Stereotactic body radiotherapy (SBRT) with high local dose has been applied to extra-cranial diseases such as peripheral Stage I non-small cell lung cancer (NSCLC) and has been reported to provide excellent local control (LC) and survival compatible with surgery (5,6). Recently, indications for SBRT have been extended to include lung metastases (7–9), liver metastases (10,11), adrenal gland metastases (12,13), spinal metastases (14–16), and others (17). Excellent LC has been reported in these reports, but the clinical benefits of SBRT for extra-cranial metastasis are yet to be determined. In most of these studies, SBRT was used for patients with fewer than five metastatic sites or for those in the clinical state of so-called oligometastasis (18).

The clinical state of oligometastatic disease was proposed in 1995 by Hellman and Weichselbaum (18), who hypothesized that LC of oligometastases may yield improved systemic control and prolonged survival. Niibe et al. (19–21) have also reported the state of oligometastasis/oligo-recurrence. They suggested that some oligometastasis/oligo-recurrence patients could survive for as long as the patients with primary cancer only, and thus these patients must be treated curatively. Improvements in diagnostic modalities have facilitated early detection of small metastatic lesions, both intra-cranial and extra-cranial, and have provided a sound rationale for Hellman and Weichselbaum's hypothesis. Recent clinical research has shown that some patients with recurrence or distant metastases can expect long-term survival after SBRT and SCRT (7–11,19–23). It remains uncertain whether these results are due to selection bias or some positive effect of SBRT and SCRT. A prospective randomized trial should be undertaken to answer this question, but prognostic factors to stratify the patients are not yet well understood.

In this study, we retrospectively analyzed our experience with SBRT and/or SCRT/SCRS for patients with oligometastases.

PATIENTS AND METHODS

Patient Characteristics

A database of patients who received SBRT and SCRT/SCRS at our institution was used to select the patients whose primary sites were treated by surgery or definitive radiation therapy between 1995 and 2007. There were 41 patients who had five or fewer detectable oligometastatic lesions at the time of SBRT and/or SCRT and had been treated with SBRT and/or SCRT/SCRS between 1999 and 2008. Diagnosis of the oligometastatic lesions was based on whole-body computed tomography (CT) and brain magnetic resonance imaging (MRI) findings. Fluorodeoxyglucose-positron emission tomography was performed as needed. The oligometastatic lesions were diagnosed by diagnostic radiologists during the diagnostic evaluation.

The treatment methods for the primary sites were surgery in 23 patients and definitive radiotherapy in 18. Definitive radiotherapy consisted of conventional radiotherapy in 8 patients and SBRT in 10.

There were seven patients who had previously been treated by SBRT and/or SCRT/SCRS to oligometastatic sites prior to receiving surgery or radiotherapy at their primary sites. The treatment time interval between the surgery/definitive radiation therapy to the primary sites and the initial SBRT and/or SCRT/SCRS to oligometastatic sites ranged from 1 to 4 months (median 2 months) in these seven patients. In the other 34 patients, the median treatment interval time from primary sites to oligometastatic sites was 21 months (range 0–121 months). We defined the treatment interval time from primary sites to oligometastatic sites as interval to recurrence. In this study, all analyses started from the day of SBRT and/or SCRT/SCRS to oligometastatic sites.

The patient characteristics are given in Table 1. There were 22 men and 19 women, and the median age was 66 years (range 30–82 years). The primary cancers consisted of lung cancer, head and neck cancer, breast cancer, colorectal cancer, renal cell carcinoma, renal pelvic cancer, hepatocellular carcinoma, thymic cancer and apocrine gland cancer. The study patients were separated into a favorable group (breast, colorectal, renal, thymic and apocrine gland cancer) and others, according to Rusthoven et al. (10). The primary histology was mainly adenocarcinoma. The number of oligometastatic tumors was mainly one or two tumors; there were only two patients who had three oligometastatic tumors and only one patient who had five. The sites involved with the oligometastatic lesions were the brain, lung and adrenal gland. Lung and adrenal gland metastases were treated by SBRT. There were no patients with oligometastatic liver metastases treated by SBRT at our institution. Fourteen patients were treated by chemotherapy as an adjuvant therapy or as a treatment for recurrence or metastases. No chemotherapy was administered during the treatment for oligometastases. No patients underwent surgical removal of the metastatic lesions.

There were 24 patients who had single or multiple brain metastases. Brain metastases were treated by SCRT or SCRS. According to the recursive partitioning analysis, 5, 18 and 1 patients were classified as Class I, Class II and Class III, respectively.

SCRT/SCRS Technique

Fifteen of 24 patients were treated by SCRT alone, five by SCRS alone and four by SCRS with WBRT for their brain metastases. The patients who received WBRT were randomly assigned to the group of SCRS with WBRT by the clinical trial of the Japanese Radiation Oncology Study Group (JROSG 99-1) (2). These patients were treated with 6- or 10-MV photons using a linac-based stereotactic system and were immobilized by a thermoshell in SCRT and a stereotactic frame in SCRS. The gross tumor volume (GTV) was defined based on MRI and CT images. A 1–3-mm

Table 1. Patient characteristics (41 patients)

Characteristics	Value
Age (years)	
Median	66
Range	30–82
Gender (*n*)	
Male	22
Female	19
Primary cancer (*n*)	
Lung	25
Head and neck	6
Breast	3
Colorectal	2
Liver	1
Renal	1
Renal pelvic	1
Thymic	1
Apocrine gland	1
Primary histology (*n*)	
Adenocarcinoma	23
Squamous cell carcinoma	6
Thyroid cancer	2
Large cell carcinoma	2
Others	8
Treatment for primary cancer (*n*)	
Resection	23
SBRT	10
Conventional radiation therapy	8
Sites involved with oligometastatic disease (no. of tumors)	
Brain	33
Lung	22
Adrenal gland	5
Number of oligometastatic tumors (*n*)	
1	27
2	11
3	2
4	0
5	1
Number of oligometastatic involved organs (*n*)	
1	37
2	4

SBRT, stereotactic body radiotherapy.

margin was added to the GTV to create the planning target volume (PTV). Treatment was prescribed to the 100% isodose line, with the 80–90% isodose line covering the PTV. A total dose of 15–25 Gy was administered in one fraction for SCRS, and a total dose of 20–40 Gy was administered in four fractions for SCRT. A total dose of 30 Gy was administered in 10 fractions for WBRT.

SBRT Technique

All patients with lung metastases and 10 patients with primary lung cancer received SBRT as the definitive radiotherapy. They received real-time tumor-tracking radiotherapy (RTRT). The RTRT system has been described in detail elsewhere (24,25). In brief, 1.5–2.0-mm gold markers were implanted near the tumor by means of image-guided procedures. CT scans were taken with the patients holding their breath at the end of normal expiration. The GTV was contoured in axial CT images. The clinical target volume (CTV) was defined three dimensionally as the GTV on CT with a 6–8-mm margin for primary lung cancers and was considered to be equal to the internal target volume. We treated adrenal gland metastases using the RTRT system. The CTV was defined as the GTV on CT with a 3-mm margin for adrenal gland metastases and with a 5-mm margin for lung metastases. The PTV was three dimensionally defined as the CTV plus a 5-mm margin with optimal reduction near the organ at risk.

Treatment was prescribed to the 100% isodose line covering the PTV within the 80% isodose line. Patients were treated with 4-, 6- or 10-MV photons. SBRT was delivered by using multiple non-coplanar static ports. A total dose of 48 Gy was administered in eight fractions in patients with adrenal gland metastases. A total dose of 35–60 Gy was administered in four or eight fractions in patients with lung metastases or primary lung cancer, respectively.

Statistical Analysis

LC was defined as no progression of the tumor in the CTV, and marginal recurrence was counted as local failure in this study. Follow-up of the patients was based on clinical examination in the outpatient clinic and/or periodic radiological examination. In principle, radiological examinations such as chest X-ray, whole-body CT and brain MRI were performed once every 3–4 months, but the frequency strongly depended on the clinical situation. The overall survival (OS) and progression-free survival (PFS) rates were calculated from the day of SBRT and/or SCRT/SCRS to oligometastatic sites using the Kaplan–Meier method.

Possible prognostic factors were as follows: age, gender, primary cancer, primary histology, treatment for primary cancer, sites involved with oligometastatic disease, number of oligometastatic tumors and the treatment interval time from primary sites to oligometastatic sites (defined as interval to recurrence). The log-rank test was used to calculate the statistically significant differences. A value of $P < 0.05$ was considered to be statistically significant. Significant variables on univariate analysis (UVA) were tested with

multivariate analyses (MVA). MVA was performed using a Cox proportional hazards regression model.

RESULTS

Local Tumor Response and Distant Metastases

The median follow-up period was 20 months (range 1–111 months). The 3- and 5-year LC rates were each 80%, and the 3- and 5-year distant control (DC) rates were each 35% (Fig. 1).

Survival

The 3-year OS and PFS rates were 39% and 20%, respectively; and the respective 5-year rates were 28% and 20% (Fig. 2). The median survival time (MST) was 24 months. Patients with adrenal gland metastasis had an MST of 15 months.

Age, primary histology and the number of oligometastatic tumors were not found to be statistically significant prognostic factors for the OS rate; however, gender, primary cancer, treatment for primary cancer, oligometastatic lung disease and interval to recurrence were statistically significant prognostic factors for the OS rate in the UVA shown in Table 2.

The OS of female patients was significantly longer than that of male patients ($P = 0.01$), and the OS of patients who had undergone resection for primary cancer was significantly longer than those of others ($P = 0.0006$). For patients with primary cancer from favorable primary sites ($n = 8$), the 3- and 5-year OS rates were both 86%, compared with 27% and 17%, respectively, for patients with primary cancer from other primary sites ($n = 33$, $P = 0.02$). We separated the patients into two groups according to interval to recurrence of <12 or ≥ 12 months ($n = 18$, 23, respectively). The 3- and 5-year OS rates were 19% and 10%, respectively, for those with an interval to recurrence of <12 months, compared with 53% and 40%, respectively, for those with an interval to recurrence of ≥ 12 months (Fig. 3; $P = 0.006$). For patients with oligometastatic lung disease with or without brain/adrenal metastases ($n = 16$), the 3- and 5-year OS rates were both 63%, compared with 22% and 14%, respectively, for patients with only brain/adrenal metastases ($n = 25$) (Fig. 4; $P = 0.009$). MVA showed no statistically significant prognostic factors for the OS rate.

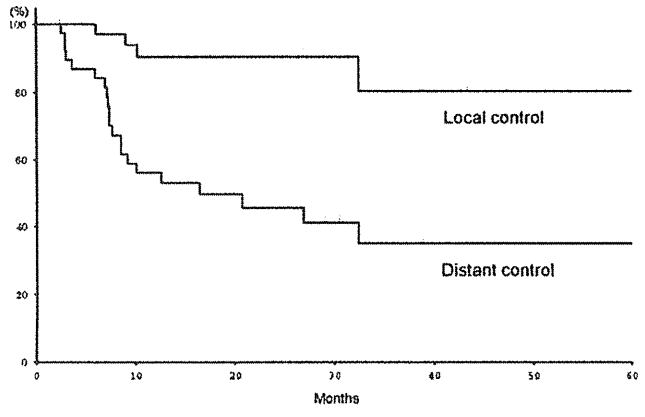

Figure 1. Kaplan–Meier actuarial local control and distant control rate.

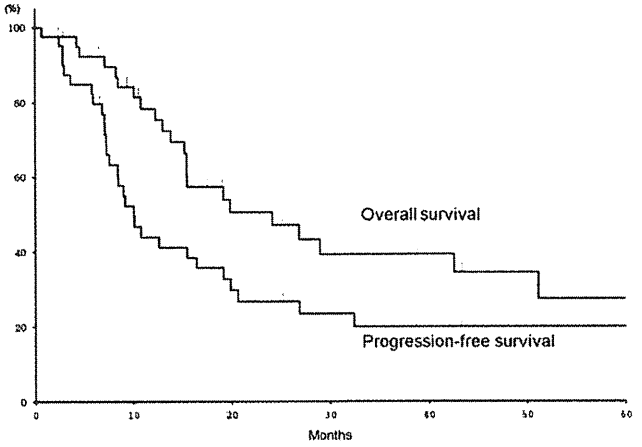

Figure 2. Kaplan–Meier actuarial overall survival (OS) and progression-free survival rate.

Table 2. UVA and MVA for OS rate

Variables	*P* value	
	UVA	MVA
Age		
<65 years	0.72	
Gender		
Female[a]	0.01*	0.72
Primary cancer		
Favorable[a]	0.02*	0.37
Primary histology		
Adenocarcinoma	0.84	
Treatment for primary cancer		
Resection[a]	0.0006*	0.26
Sites involved with oligometastatic disease		
Brain	0.09	
Lung	0.009*	0.47
Adrenal gland	0.09	
Number of oligometastatic tumors		
Single metastasis	0.47	
Interval to recurrence		
≥12 months[a]	0.006*	0.52

UVA, univariate analysis; MVA, multivariate analysis; OS, overall survival.
*Significant ($P < 0.05$).
[a]These variables were favorable predictors for overall survival rate on UVA.

Long Survivors

Four 5-year survivors consisted of two with lung adenocarcinoma, one with renal pelvic cancer and one with thymic cancer. One patient with lung adenocarcinoma had one brain metastasis treated by SCRT, whereas the other patient with lung adenocarcinoma had one brain metastasis treated by SCRS with WBRT and one lung metastasis treated by SBRT. The patient with renal pelvic cancer had two lung metastases treated by SBRT, and the patient with thymic cancer had one lung metastasis treated by SBRT.

Toxicities

Adverse effects were graded according to the Common Toxicity Criteria for Adverse Events, version 3.0. Grade 2 complications occurred in four patients (9.8%), radiation necrosis of the brain occurred in three patients and intercostal neuralgia occurred in one patient. No other adverse effects of Grade 2 or more were observed.

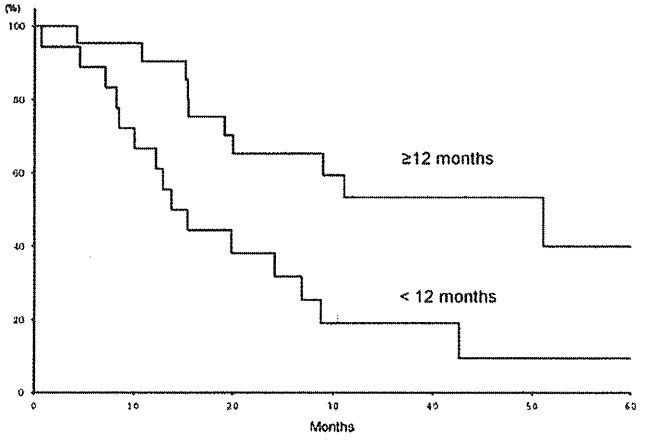

Figure 3. Kaplan–Meier curve of OS rates for patients with interval to recurrence of <12 months ($n = 18$) and ≥ 12 months ($n = 23$). Significant statistical difference was found ($P = 0.006$) between the two groups.

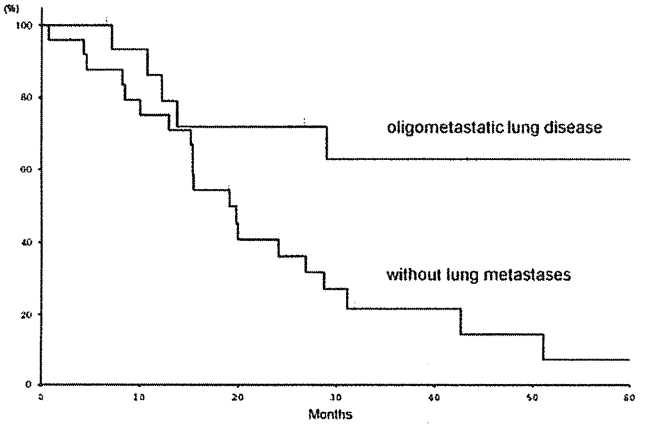

Figure 4. Kaplan–Meier curve of OS rates for patients with oligometastatic lung disease with or without brain/adrenal metastases ($n = 16$) and only brain/adrenal metastases ($n = 25$). Significant statistical difference was found ($P = 0.009$) between the two groups.

DISCUSSION

In this study, the OS rates at 3 and 5 years were 39% and 28%, respectively, and the MST was 24 months, which is equivalent to that in the study of oligometastases previously published, as follows. Milano et al. (22) reported the results of a Phase II trial using SBRT to a dose of 50 Gy in 10 fractions in the treatment of oligometastatic disease with 4-year OS, PFS, LC and DC rates of 28%, 20%, 60% and 25%, respectively. Patients with breast cancer fared significantly better with respect to OS, PFS, LC and DC rates (26), and those with adrenal metastases had significantly worse OS, LC and DC rates (13).

Rusthoven et al. (9,10) have recently reported the results of multi-institutional Phase I/II trials of SBRT for lung and liver metastases. The actual LC rate at 1 and 2 years after SBRT for oligometastatic lung tumors were 100% and 96%, respectively, and the MST was 19 months. The actual in-field LC rates at 1 and 2 years after SBRT for oligometastatic liver tumors were 95% and 92%, respectively, and the MST was 20.5 months. The primary tumor site was significantly predictive of survival. Primary tumors of the lung and ovary as well as non-colorectal gastrointestinal malignancies were found to be associated with poorer survival compared with breast, colorectal, renal, carcinoid and gastrointestinal stromal tumors as well as sarcoma.

Flannery et al. (23) have reported long-term survival in patients with synchronous solitary brain metastasis from NSCLC treated with radiosurgery. The MST was 18 months, and the 1-, 2- and 5-year actuarial OS rates were 71.3%, 34.1% and 21%, respectively. For patients who underwent definitive thoracic therapy, the 5-year actuarial OS rate was 34.6% compared with 0% for those who had non-definitive therapy. The Karnofsky performance status (KPS) also significantly impacted the OS rate.

SBRT and SCRT have been applied for the treatment of metastatic lesions recently; however, conventional radiotherapy remains a standard option for the treatment of metastatic lesions. Andrews et al. (4) reported the result of a Phase III study that compared WBRT with or without SCRS for brain metastases. This study showed WBRT with SCRS improved survival for patients with single brain metastasis or patients with tumors > 2.0 cm in diameter. To our knowledge, there has been no study that compared SBRT with conventional radiotherapy for extra-cranial metastases.

It is important to find prognostic factors related to long-term survival after definitive therapy such as SBRT and SCRT for oligometastatic lesions. According to the studies described above, KPS, the primary tumor site and the oligometastatic site can be predictive of survival. Low KPS, a primary tumor site such as the lung and adrenal metastasis were found to be associated with lower survival in the

previous study (9,10,13,22,23,26). However, our results have shown that some patients with lung cancer can survive >5 years after treatment for oligometastases and that some with adrenal metastatic tumors can expect an MST of 15 months. These findings are consistent with those of Khan et al. (27). It would therefore be useful to find prognostic factors that are independent of the primary and metastatic sites.

In this study, we identified another factor that can be used to predict long-term survival. The treatment interval time from primary sites to oligometastatic sites, defined as interval to recurrence, was found to be significantly associated with the OS rate in the UVA. A long interval to recurrence implies that the patient has a slowly growing tumor or is under good control with regard to primary and other sites except for the apparent metastatic lesions. In contrast, a short interval to recurrence indicates rapid tumor growth or poor control of the primary and other metastatic sites. Although it was difficult to distinguish between the natural course of the disease and the effects of treatment in this retrospective study, interval to recurrence was shown to be an independent parameter to predict prognosis for patients with oligometastases.

The clinical state of oligometastatic disease was proposed in 1995 by Hellman and Weichselbaum (18), but a clear definition for oligometastasis has not yet been established. Table 3 shows various definitions of oligometastasis reported previously in the literature. The number of oligometastases ranges from 1 to 6 tumors. Oligometastatic lesions are mainly in the lung, liver and brain, although oligometastases in the bone, adrenal gland, lymphatic nodes and soft tissue have also been reported. In the present study, we defined the number of oligometastases as ranging from 1 to 5 tumors, and oligometastatic lesions were found in the lung, brain and adrenal gland, which is consistent with several previous reports. A definitive definition of oligometastasis may not be possible, due to its diverse nature, but a clear definition is required for further investigation.

Table 3. Definition of oligometastasis

	Number of patients	Oligometastases	Oligometastatic lesions
Norihisa et al. (8)	34	1–2	Lung
Rusthoven et al. (9)	38	1–3	Lung
Rusthoven et al. (10)	47	1–3	Liver
Katz et al. (11)	69	1–6	Liver
Rades et al. (14)	521	1–3	Vertebrae
Salama et al. (17)	29	1–5	Lung, node, liver, bone, soft tissue, adrenal gland
Milano et al. (22)	121	1–5	Lung, node, liver, brain, adrenal gland, bone
Flannery et al. (23)	42	1	Brain
Khan et al. (27)	23	1–2	Lung, brain, soft tissue, adrenal gland, bone
Current study	41	1–5	Lung, brain, adrenal gland

One shortcoming of this paper is the retrospective nature of the analysis. Patients with sufficient medical conditions were probably selected beforehand to receive SBRT and SCRT. The large number of patients who died within a short period may have masked the possible progression of the disease and local failure. However, it is notable that there is a definite group of patients treated with SBRT and SCRT who experienced long survival even with distant metastasis. A large prospective trial is required to investigate the actual benefits of SBRT and SCRT for patients with oligometastases. Our findings suggest that interval to recurrence should be included in the stratification criteria in a prospective randomized trial comparing treatment with or without SBRT and SCRT.

In conclusion, precise SBRT and SCRT were effective in controlling oligometastatic lesions for patients with an MST of 24 months. Interval to recurrence may impact the OS rate and should be included in the stratification criteria of a prospective randomized trial to investigate the benefits of SBRT and SCRT for patients with oligometastases.

Conflict of interest statement

None declared.

References

1. Aoyama H, Shirato H, Onimaru R, Kagei K, Ikeda J, Ishii N, et al. Hypofractionated stereotactic radiotherapy alone without whole-brain irradiation for patients with solitary and oligo brain metastasis using noninvasive fixation of the skull. *Int J Radiat Oncol Biol Phys* 2003;56:793–800.
2. Aoyama H, Shirato H, Tago M, Nakagawa K, Toyoda T, Hatano K, et al. Stereotactic radiosurgery plus whole-brain radiation therapy vs stereotactic radiosurgery alone for treatment of brain metastases: a randomized controlled trial. *JAMA* 2006;295:2483–91.
3. Sperduto PW, Berkey B, Gaspar LE, Mehta MCurran W. A new prognostic index and comparison to three other indices for patients with brain metastases: an analysis of 1960 patients in the RTOG database. *Int J Radiat Oncol Biol Phys* 2008;70:510–4.
4. Andrews DW, Scott CB, Sperduto PW, Flanders AE, Gaspar LE, Schell MC, et al. Whole brain radiation therapy with or without stereotactic radiosurgery boost for patients with one to three brain metastases: phase III results of the RTOG 9508 randomised trial. *Lancet* 2004;3:1665–72.
5. Onishi H, Shirato H, Nagata Y, Hiraoka M, Fujino M, Gomi K, et al. Hypofractionated stereotactic radiotherapy (HypoFXSRT) for stage I non-small cell lung cancer: updated results of 257 patients in a Japanese multi-institutional study. *J Thorac Oncol* 2007;2:S94–100.
6. Baumann P, Nyman J, Hoyer M, Wennberg B, Gagliardi G, Lax I, et al. Outcome in a prospective phase II trial of medically inoperable stage I non-small-cell lung cancer patients treated with stereotactic body radiotherapy. *J Clin Oncol* 2009;20:3290–6.
7. Okunieff P, Petersen AL, Philip A, Milano MT, Katz AW, Boros L, et al. Stereotactic body radiation therapy (SBRT) for lung metastases. *Acta Oncol* 2006;45:808–17.

8. Norihisa Y, Nagata Y, Takayama K, Matsuo Y, Sakamoto T, Sakamoto M, et al. Stereotactic body radiotherapy for oligometastatic lung tumors. *Int J Radiat Oncol Biol Phys* 2008;72:398–403.
9. Rusthoven KE, Kavanagh BD, Burri SH, Chen C, Cardenes H, Chidel MA, et al. Multi-institutional phase I/II trial of stereotactic body radiation therapy for lung metastases. *J Clin Oncol* 2009;27:1579–84.
10. Rusthoven KE, Kavanagh BD, Cardenes H, Stieber VW, Burri SH, Feigenberg SJ, et al. Multi-institutional phase I/II trial of stereotactic body radiation therapy for liver metastases. *J Clin Oncol* 2009;27:1572–8.
11. Katz AW, Carey-Sampson M, Muhs AG, Milano MT, Schell MC, Okunieff P. Hypofractionated stereotactic body radiation therapy (SBRT) for limited hepatic metastases. *Int J Radiat Oncol Biol Phys* 2007;67:793–8.
12. Katoh N, Onimaru R, Sakuhara Y, Abo D, Shimizu S, Taguchi H, et al. Real-time tumor-tracking radiotherapy for adrenal tumors. *Radiother Oncol* 2008;87:418–24.
13. Chawla S, Chen Y, Katz AW, Muhs AG, Philip A, Okunieff P, et al. Stereotactic body radiotherapy for treatment of adrenal metastases. *Int J Radiat Oncol Biol Phys* 2009;75:71–5.
14. Rades D, Veninga T, Stalpers LJ, Basic H, Rudat V, Karstens JH, et al. Outcome after radiotherapy alone for metastatic spinal cord compression in patients with oligometastases. *J Clin Oncol* 2007;25:50–6.
15. Yamada Y, Bilsky MH, Lovelock DM, Venkatraman ES, Toner S, Johnson J, et al. High-dose, single-fraction image-guided intensity-modulated radiotherapy for metastatic spinal lesions. *Int J Radiat Oncol Biol Phys* 2008;71:484–90.
16. Sahgal A, Ames C, Chou D, Ma L, Huang K, Xu W, et al. Stereotactic body radiotherapy is effective salvage therapy for patients with prior radiation of spinal metastases. *Int J Radiat Oncol Biol Phys* 2009;74:723–31.
17. Salama JK, Chmura SJ, Mehta N, Yenice KM, Stadler WM, Vokes EE, et al. An initial report of a radiation dose-escalation trial in patients with one to five sites of metastatic disease. *Clin Can Res* 2008;14:5255–9.
18. Hellman S, Weichselbaum RR. Oligometastases. *J Clin Oncol* 1995;13:8–10.
19. Niibe Y, Kazumoto T, Toita T, Yamazaki H, Higuchi K, Ii N, et al. Frequency and characteristics of isolated para-aortic lymph node recurrence in patients with uterine cervical carcinoma in Japan: a multi-institutional study. *Gynecol Oncol* 2006;103:435–8.
20. Niibe Y, Kenjo M, Kazumoto T, Michimoto K, Takayama M, Yamauchi C, et al. Multi-institutional study of radiation therapy for isolated para-aortic lymph node recurrence in uterine cervical carcinoma: 84 subjects of a population of more than 5,000. *Int J Radiat Oncol Biol Phys* 2006;66:1366–9.
21. Niibe Y, Kuranami M, Matsunaga K, Takaya M, Kakita S, Hara T, et al. Value of high-dose radiation therapy for isolated osseous metastasis in breast cancer in terms of oligo-recurrence. *Anticancer Res* 2008;28:3929–31.
22. Milano MT, Katz AW, Muhs AG, Philip A, Buchholz DJ, Schell MC, et al. A prospective pilot study of curative-intent stereotactic body radiation therapy in patients with 5 or fewer oligometastatic lesions. *Cancer* 2008;112:650–8.
23. Flannery TW, Suntharalingam M, Regine WF, Chin LS, Krasna MJ, Shehata MK, et al. Long-term survival in patients with synchronous, solitary brain metastasis from non-small-cell lung cancer treated with radiosurgery. *Int J Radiat Oncol Biol Phys* 2008;72:19–23.
24. Shirato H, Shimizu S, Kunieda T, Kitamura K, van Herk M, Kagei K, et al. Physical aspects of a real-time tumor-tracking system for gated radiotherapy. *Int J Radiat Oncol Biol Phys* 2000;48:1187–95.
25. Shirato H, Shimizu S, Kitamura K, Nishioka T, Kagei K, Hashimoto S, et al. Four-dimensional treatment planning and fluoroscopic real-time tumor tracking radiotherapy for moving tumor. *Int J Radiat Oncol Biol Phys* 2000;48:435–42.
26. Milano MT, Zhang H, Metcalfe SK, Muhs AG, Okunieff P. Oligometastatic breast cancer treated with curative-intent stereotactic body radiation therapy. *Breast Cancer Res Treat* 2009;115:601–8.
27. Khan AJ, Mehta PS, Zusag TW, Bonomi PD, Penfield Faber L, Shott S, et al. Long term disease-free survival resulting from combined modality management of patients presenting with oligometastatic, non-small cell lung carcinoma (NSCLC). *Radiother Oncol* 2006;81:163–7.

Radiol Phys Technol (2010) 3:16–22
DOI 10.1007/s12194-009-0071-4

A parameter study of pencil beam proton dose distributions for the treatment of ocular melanoma utilizing spot scanning

Kenneth Sutherland · Satoshi Miyajima · Hiroyuki Date · Hiroki Shirato · Masayori Ishikawa · Masao Murakami · Mitsuru Yamagiwa · Paul Bolton · Toshiki Tajima

Received: 7 April 2009 / Revised: 4 August 2009 / Accepted: 4 August 2009 / Published online: 19 September 2009

Abstract The results of Monte Carlo calculated dose distributions of proton treatment of ocular melanoma are presented. An efficient spot scanning method utilizing active energy modulation, which also minimizes the number of target spots was developed. We simulated various parameter values for the particle energy spread and the pencil beam diameter in order to determine values suitable for medical treatment. We found that a 2.5-mm-diameter proton beam with a 5% Gaussian energy spread was suitable for treatment of ocular melanoma while preserving vision for the typical case that we simulated. The energy spectra and the required proton current were also calculated and are reported. The results are intended to serve as a guideline for a new class of low-cost, compact accelerators.

K. Sutherland (✉) · H. Date · H. Shirato · M. Ishikawa
Hokkaido University School of Medicine,
Kita-ku Kita 12 Jo Nishi 5 Chome,
Sapporo 060-0812, Japan
e-mail: kensuth@med.hokudai.ac.jp

K. Sutherland · S. Miyajima
Japan Science and Technology,
Motomachi 4 Chome 1 Ban 8 Go,
Kawaguchi, Saitama 332-0012, Japan

M. Yamagiwa · P. Bolton · T. Tajima
Photo-Medical Research Center, Japan Atomic Energy Agency,
Kizugawa, Kyoto 619-0215, Japan

M. Murakami
Hyogo Ion Beam Medical Center,
Shinguu Chou Hikarimiya 1-2-1,
Tatsuno, Hyogo, Japan

Keywords Proton therapy · Ocular melanoma · Monte Carlo simulation · Laser acceleration

1 Introduction

Proton beams have the potential to decrease normal tissue damage and allow dose escalation in cancer therapy, because the beam profile allows a more localized dose distribution at the tumor than do traditional X-rays. For covering the volume of a target lesion in particle therapy for cancer, two methods have been employed: passive scattering and spot scanning. In the passive scattering method, secondary neutrons from scatter foils, compensators and collimators are a possible source of secondary malignancy [1]. Spot scanning was first proposed as an alternative to passive scattering methods by Kanai et al. [2] and was further investigated by Lomax et al. [3]. Spot scanning utilizes magnetic and mechanical scanning of a pencil proton beam such that individually weighted Bragg peaks are distributed under computer control [4]. For spot scanning, there is no need for patient-specific collimators, thereby reducing the whole-body neutron dose to the patient. Another advantage is that most of the particles from the accelerator can be delivered to the patient, rather than being absorbed by collimators or compensators, and therefore this method is potentially more efficient.

In this work, we present the results of Monte Carlo simulations of proton dose distributions in which we used parameterized proton beams applied to ocular melanoma. We hope that the results of this study will serve as a guide for researchers developing proton facilities for medical treatment. We comment on the potential relevance of laser-accelerated protons [5–8] for the treatment of ocular melanoma, which requires lower proton energies than do more

deeply seated tumors, as well as relatively lower doses (fewer protons) because such tumors are typically small. However, the results should be applicable to proton therapy in general.

2 Materials and methods

2.1 Monte Carlo simulation speed improvements

Geant4 [9] version 8.0p1 was used for these simulations. Geant4 has been validated previously for medical-physics applications [10]. In order to improve the execution speed, we modified the particle navigation library following Jiang and Paganetti [11]. To improve efficiency on a PC cluster, we also developed a custom parallelization of Geant4 [12]. Simulations yield exactly the same results when running in parallel on a cluster or on a single processor as long as random-number-generator seed values are maintained and are set at the beginning of each event.

Following Jiang and Paganetti [11], four physics processes were registered in the Geant4 physics list for proton interactions: proton elastic scattering (*G4HadronElasticProcess*), proton inelastic scattering (*G4HadronInelasticProcess*), ionization (*G4hLowEnergyIonisation*) and multiple scattering (*G4MultipleScattering*). For improved efficiency, only secondary protons and neutrons were tracked. The energy from secondary electrons was deposited locally because the range was assumed to be less than 1 mm in water. The Geant4 maximum step size was limited to 1 mm.

2.2 Radiation treatment simulation software

We developed an application, which investigates the effects of the proton beam diameter and energy spread on the dose distribution. The software allows the user to open a series of DICOM CT images, and specify the target volume, one or more gantry positions and various beam characteristics. The user can also enter the particle (i.e., event) count. We chose a particle count of 1 million for this study, which we determined to be sufficient for good energy deposit distribution statistics with a reasonable processing time.

We used a series of 11 CT images of a disease-free human head with a slice thickness of 2.5 mm and a pixel spacing of 0.3125 mm. The CT pixel value (in Hounsfield units) of each voxel was used for determining the voxel material. Each material was assigned a density and a chemical composition according to the data provided by Schneider et al. [13]. The software generates files, which specify the different voxel materials and an event list containing the initial source position, direction and energy of each particle in the simulation. The dose accumulation grid had the same size and dimensions as the CT data: 512 × 512 × 11; i.e., we did not subsample or smoothen the CT values.

A database of depth and lateral dose profile curves was pre-computed with the use of the Monte Carlo package *Particle and Heavy Ion Transport Code System* (PHITS) [14, 15]. This database was used by our planning software for determining the initial energy peak, energy spread and spot spacing. Depth–dose curves were computed for proton beams incident on water with energies from 30 to 250 MeV in 1-MeV increments. Four values of the Gaussian energy spread were computed: 0, 5, 10 and 15%, at a depth resolution of 0.1 mm. Lateral offset tables were computed for energies from 30 to 200 MeV in 1-MeV increments, with the use of the same energy spread values, 0, 5, 10, and 15%, and with beam diameters of 0, 1.25, 2.5, 5 and 10 mm. The tables were stored in a binary format, which minimized the time necessary for reading of the data by the planning software.

An initial weighting factor was assigned to each target spot, which was used for determining the particle count. The deepest spot (associated with the highest energy) along a beam is assigned weight 1.0. Shallower spots are then assigned weights less than 1.0 based on the pre-computed database of dose distribution curves to achieve a spread-out Bragg peak (SOBP). The target weight is then used with the total particle count for assignment of individual particle counts for each target spot. At this step, the energy spread and beam diameter are factored in by addition of small random values to the initial energy and position of each particle. In the case of the energy spread, random numbers are chosen so that the resulting particle energies have a Gaussian distribution with the specified full width at half maximum (FWHM). Another pair of random numbers is chosen to place the particle within the specified beam diameter. Particles are distributed evenly along the beam axis. The particle list is then written on a file, which is read by the simulation program.

2.3 Target spot spacing

We incorporated a spot scanning method where the beam position and direction were fixed, while target spots along the beam direction were scanned by depth variation; i.e., active energy variation for depth modulation. All beams are assumed to be parallel to each other in this simulation (Fig. 1). This method requires a rapid alteration of the proton energy.

Our software also has the ability automatically to place target spots at locations with variable spacing based on the pre-computed database of dose profile curves in water. In the case of lateral spacing, lateral fall-off curves at the

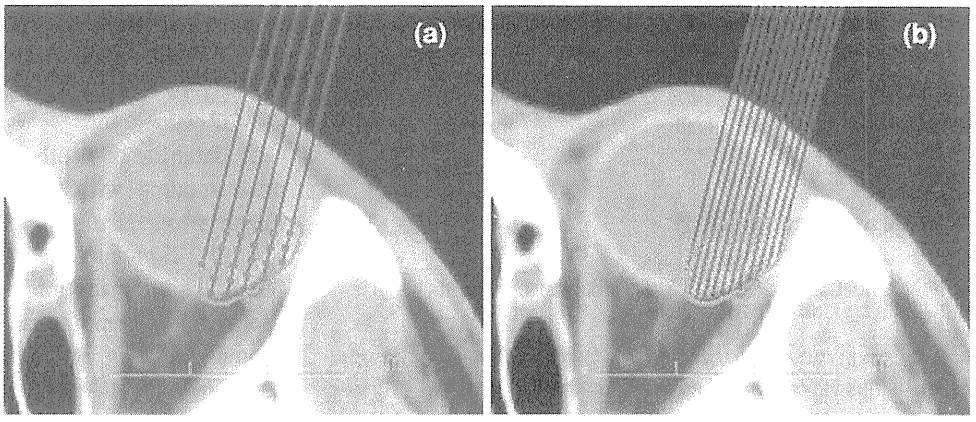

Fig. 1 Effect of beam parameters on target spot placement and beam spacing. *Blue lines* are beams. The *green polygon* is the planned target volume (PTV). *Red dots* are target spots. a 5-mm beam diameter and 10% energy spread. b 1.25-mm beam diameter and 0% energy spread, for which more target spots are generated (color figure online)

beam's pre-computed Bragg peak depth are used for determining the width (FWHM) of the beam, specifying a "spot width". The spot width is mostly affected by the beam diameter and by lateral scatter. For depth spacing, the beam's pre-computed depth–dose profile curve was used similarly for specifying a "spot depth". The spot depth is affected mostly by the energy spread.

Utilizing spot width and depth alone for spot spacing results in an uneven dose distribution within the target region due to under-dosed regions between spots. For achieving a smooth dose distribution, the spot width and the spot depth are multiplied by a "spacing factor". The spacing factor is usually less than 1.0 and has the effect of placing the spots closer together, i.e., increasing the number of spots. A spacing factor of 0.5, which we found yields a relatively smooth dose distribution while minimizing the number of target spots, was used throughout this simulation. A more detailed examination of the effect of the spacing factor on the dose distribution and the number of spots is a topic for future investigation.

2.4 Dose distribution optimization

It is difficult to predict the exact dose distribution in inhomogeneous patient volumes based on CT data alone. Therefore, after the initial Monte Carlo simulation, we fine-tuned the particle counts assigned to each target spot in the following way. The dose distribution for each target spot is calculated with the Monte Carlo simulation program and stored in separate files, one dose distribution file per target spot. The individual files are read and summed to form a complete dose distribution. The dose deposited at each target spot is compared with the dose average in the planning target volume (PTV). Spots that received less than the average dose (cold spots) are assigned more particles, and spots with a higher dose (hot spots) are assigned fewer particles. The process is repeated iteratively until it is determined that the result cannot be optimized further. Note that we do not attempt to reduce the dose deposited in critical structures; we only attempt to achieve a uniform dose distribution within the target volume in this optimization process.

2.5 Target polygon

The gross target volume (GTV) was modeled as a semi-ellipsoid with a semi-sphere base of height 4.8 mm and basal diameter 13 mm. The minimum tumor–optic disk distance was 5 mm. The tumor–macula distance was 4 mm. The values were chosen to represent a typical tumor based on data reported by Dendale et al. [16]. The GTV was generated in the planning software by specification of the tumor height, base diameter, eye center and tumor base position. A 2-mm margin was automatically added to the perimeter of the GTV to form the PTV. The volume of the PTV was .734 cm^3. The target polygon (PTV) and organs at risk (OARs) are shown in Fig. 2.

The prescribed dose was set to 54.5 Gy, which is equal to 60 cobalt Gray equivalent (CGE), assuming a relative radiobiological effectiveness (RBE) of 1.1. The tumor was assumed to be free of infiltration of the optic disk or macula. The dose distribution was normalized so that ninety-five percent of the PTV received at least 100% of the prescribed dose; i.e., "D95" for the PTV was set to 60 CGE. Four fractions in one week were assumed to be used, which is the common practice in conventional proton therapy. The effects of the energy spread and beam diameter were investigated with 60 CGE kept for D95 in each calculation.

3 Results

In the first series of simulations, the effect of the energy spread of the beam on the dose distribution was investigated. Energy spread values of 5, 10 and 15% were simulated. The beam diameter was 2.5 mm in each case. Dose distributions are shown in Fig. 3. Dose–volume

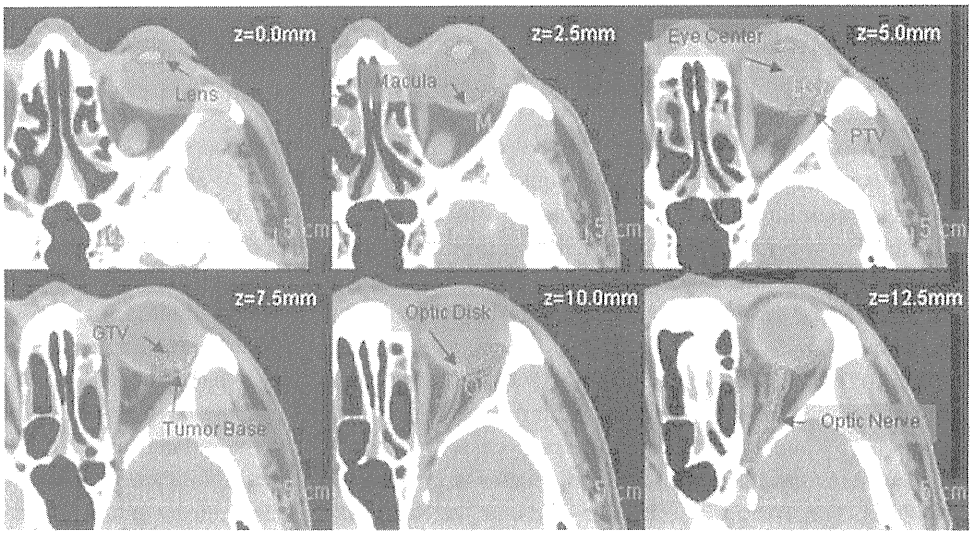

Fig. 2 Target polygons and organs at risk (OARs) used for this experiment. The inner target polygon is the *GTV*. The GTV is generated automatically by specifying the location of the tumor base and eye center. The size of the GTV is determined by specifying the basal diameter and tumor height. The outer target polygon is the *PTV* (GTV plus 2-mm margin). OARs include the lens, optic nerve macula, and optic disk (color figure online)

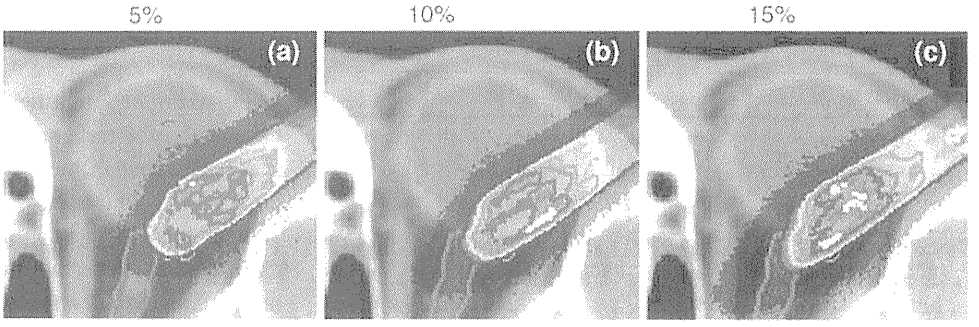

Fig. 3 Dose distributions for various values of energy spread. 5% (a), 10% (b) and 15% (c). Isodose lines are 125% of prescribed dose (75 CGE) *white*, 110% (66 CGE) *red*, 90% (54 CGE) *orange*, 75% (45 CGE) *yellow*, and 50% (30 CGE) *blue*. In all cases, a 2.5-mm beam width was used (color figure online)

histograms (DVHs) are shown in Fig. 4, and simulation results are summarized in Table 1. The table indicates that, at 5% energy spread, the dose to the macula and optic disc was below the tolerance values for the case that we simulated. At 10 and 15%, it was difficult to preserve critical structures located behind the distal edge of the target volume due to the elongated fall-off of the depth profile curve.

Target spot and beam characteristics are summarized in Table 2. The table shows the effect of energy spread (5, 10 and 15%) on the depth spacing and the number of target spots with a constant beam diameter (2.5 mm). The depth spacing (the distance between target spots along a beam) is increased with increasing energy spread, whereas the number of target spots is decreased with increasing energy spread.

In the second series, the effect of the beam diameter on the dose distribution was investigated. Beam diameter values of 1.25, 2.5 and 5 mm were simulated. The energy spread value for each case was 5%. Dose distributions are shown in Fig. 5, and DVHs are shown in Fig. 6. Figure 5 illustrates that the volume of hot spots in the PTV increased when the beam diameter was increased from 1.25to 2.5 mm. The simulation results are summarized in Table 3.

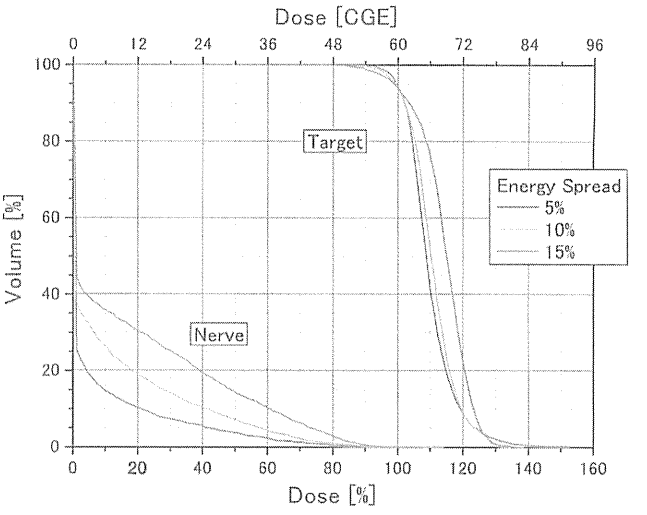

Fig. 4 DVH of PTV and optic nerve for various energy spread values. In all cases a 2.5-mm beam diameter was used (color figure online)

The table indicates that a beam diameter of less than or equal to 2.5 mm would not exceed the tolerance doses for the case that we studied. At 5-mm beam diameter, the dose to the lens becomes significant.

Table 4 indicates the effect of the beam diameter (1.25, 2.5 and 5 mm) with a fixed energy spread of 5%. The maximum and minimum values of the depth spacing were almost constant, as anticipated from the fixed energy spread. Also, the beam diameter affected the lateral spacing, as expected. The number of beams and target spots decreased significantly with an increase in the beam diameter. For a beam of 1.25 mm, nearly a thousand target spots were generated by the planning software. Such a large number of target spots would likely require a lot of time to treat.

A histogram of particle energy for a typical treatment plan is displayed in Fig. 7. In general, more particles at the higher-energy end of the spectrum are necessary because more particles are targeted at deeper locations in forming the SOBP. The energy distribution is also affected by the target shape and the incident beam direction. The energy distribution is not smooth, partly due to the discrete proton energy values used for our calculations.

Table 1 Dosimetric characteristics: energy spread

Energy spread	5%	10%	15%
Retina ≥45 CGE	1%	2%	5%
Lens ≥10 CGE	0%	0%	0%
Optic nerve ≥12 CGE	10%	20%	31%
Dose at macula (≥30 CGE)	27 (OK)	36 (NG)	42 (NG)
Dose at optic disc (≥12 CGE)	11 (OK)	1.8 (OK)	3.3 (OK)
V95[a]	98%	98%	97%

[a] Percentage volume of PTV, which received 95% of the prescribed dose (57 CGE)

Table 2 Target spot and beam characteristics: energy spread

Energy spread	5%	10%	15%
Lateral spacing (mm)	1.3	1.3	1.3
Depth spacing, minimum (mm)	0.6	1.7	3.1
Depth spacing, maximum (mm)	2.8	5.8	9.1
Number of beams	38	38	38
Number of target spots	239	102	65

Beamlet diameter was 2.5 mm for each case

4 Discussion

Many parameters and parameter combinations (such as beam diameter, energy spread, lateral spacing, depth spacing, number of beams and number of target spots) must be considered in assessing proton treatment of small superficial tumors. Realistically, some of the parameters may need to be predetermined in the clinical equipment because of mechanical or other limitations. In this study, we simulated the effect of energy spread by using a fixed beam diameter (2.5 mm), and the effect of the beam diameter by using a fixed energy spread (5%). These values were chosen because they seemed to be the most likely parameters delivered by an actual accelerator. A more thorough parameter survey is necessary for determination of the effects of every possible combination of beam parameters.

For reducing treatment times, it is desirable to reduce the number of target spots in a plan. However, there is a trade-off between the dose distribution and the number of target spots. Our results suggest that, if the beam energy and lateral spacing are predetermined, the energy spread and beam diameters must be chosen carefully with this in mind. The clinical significance of dose–volume statistics of the PTV and organs at risk must be determined for each patient.

The dose distributions shown here contain many hot spots (overdose areas). These are caused partially by the histogram normalization method, where 95% of the target volume is forced to receive at least 100% of the prescribed dose. Without normalization, cold spots were prevalent around the lateral and distal edges, especially when a large beam diameter or energy spread was used. The cold spots became prevalent when the distance from the tumor polygon edge and nearest target spot was relatively large. This resulted in DVH curves for the target volume not being as steep (selective) as they should have been. Several methods can be employed for improving the dose distributions,

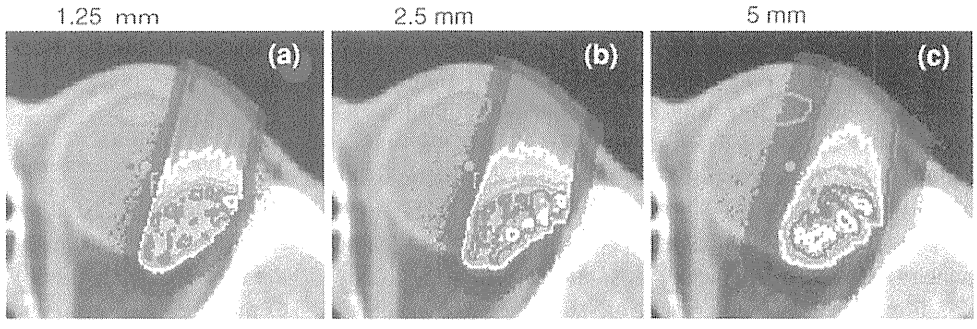

Fig. 5 Dose distribution for various values for beam diameter, 1.25 mm (**a**) 2.5 mm (**b**), and 5 mm (**c**). Isodose lines are 125% of prescribed dose (75 CGE) *white*, 110% (66 CGE) *red*, 90% (54 CGE) *orange*, 75% (45 CGE) *yellow* and 50% (30 CGE) *blue*. In all cases, we used 5% energy spread (color figure online)

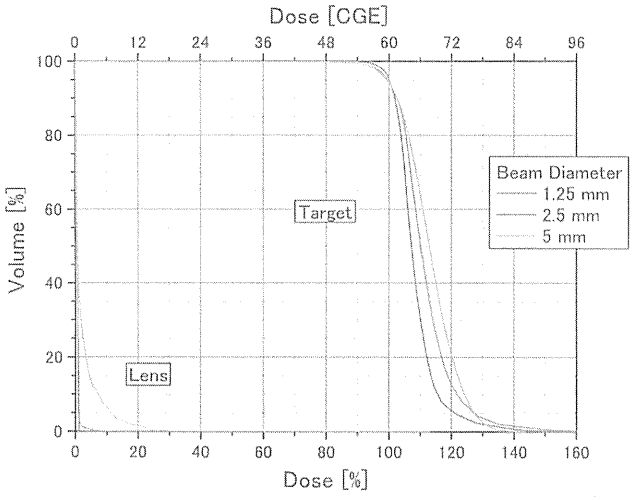

Fig. 6 DVH for PTV and optic nerve computed with various values for beam diameter. In all cases, we used 5% energy spread (color figure online)

Table 3 Dosimetric characteristics: beam diameter

Beam diameter	1.25 mm	2.5 mm	5 mm
Retina ≥45 CGE	0%	0%	1%
Lens ≥10 CGE	0%	0%	6%
Optic nerve ≥12 CGE	0%	1%	4%
Dose at macula (≥30 CGE)	13 (OK)	13 (OK)	36 (NG)
Dose at optic disc (≥12 CGE)	0.8 (OK)	3.0 (OK)	18 (NG)
V95[a]	99%	98%	98%

[a] Percentage volume of CTV, which received 95% of the prescribed dose (57 CGE)

Table 4 Spot and beam characteristics: beam diameter

Beam diameter	1.25 mm	2.5 mm	5 mm
Lateral spacing (mm)	0.7	1.4	2.6
Depth spacing, minimum (mm)	0.7	0.7	0.6
Depth spacing, maximum (mm)	2.4	2.4	2.3
Number of beams	206	57	21
Number of target spots	918	233	87

Energy spread was 5% for each case

including increasing the number of Monte Carlo events, decreasing the space between target spots and improving the optimization algorithm. Furthermore, we used a fixed spacing factor of 0.5 in this study. Introduction of a variable spacing factor for each beam may further improve the homogeneity of dose distributions. The spacing factor should be smaller near the polygon edges to prevent cold spots while maintaining a reasonable total number of spots. These are topics for future study.

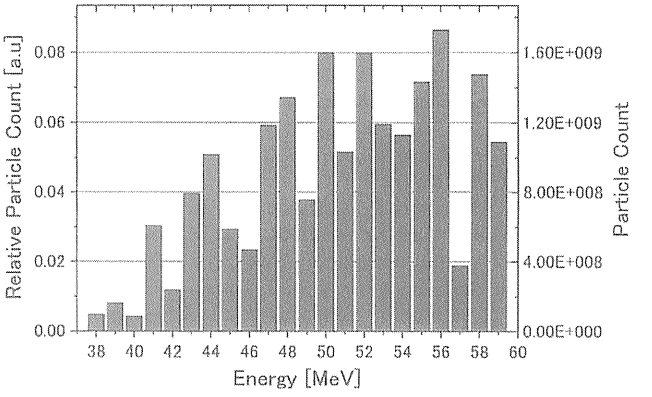

Fig. 7 A typical histogram of particle energy levels (color figure online)

In this work, doses to the macula and to the optic disc were high and above the clinical limits in some cases. This is mainly because these structures are located directly behind the distal edge of the target volume. Proton spectra that are closer to being monoenergetic may improve the final clinical outcome. The effect of energy spread for deep-seated tumors such as prostate cancer may be different from that for shallow ocular diseases and is yet to be determined.

The required proton flux can be estimated as follows. Consider a shallow tumor volume of 1 cc (1 g). If the protons deposit an average energy of 50 MeV, then each proton delivers about 8×10^{-12} J or 8×10^{-9} Gy on average. Assuming an RBE of 1.1, each proton delivers about 9×10^{-9} CGE. A typical treatment course consists of 60 CGE delivered in four fractions on consecutive days. If the irradiation time is limited to 1 min, then the accelerator must deliver 15 CGE per min or .25 CGE per s. The accelerator must therefore produce about 30 million protons per second or 4.8 pA. If such a delivery was carried out in 100 Hz repetitive pulsed laser shots, the required delivery would be in the order of 3×10^5 protons per shot.

5 Conclusion

Our simulations show that a 2.5-mm beam diameter and a 5% energy spread can be considered as a starting point for ocular cases. The dose distributions suggest that there is merit in continuing such parameter studies and considering further the potential for spot scanning proton sources.

Acknowledgments This work was supported by the Core Research for Evolutional Science and Technology (CREST), the Japan Science and Technology Agency (JST) and the Special Coordination Fund (SCF) for Promoting Science and Technology commissioned by the Ministry of Education, Culture, Sports, Science and Technology (MEXT) of Japan. K. S. is a Takuma Scholar of PMRC.

References

1. Brenner DJ, Hall EJ. Secondary neutrons in clinical proton radiotherapy: a charged issue. Radiat Oncol. 2008;86(2):165–70.
2. Kanai T, Kawachi K, Kumamoto Y, Ogawa H, Yamada Y, Matsuzawa H. Spot scanning system for proton radiotherapy. Med Phys. 1980;7(4):365–9.
3. Lomax AJ, Bohringer T, Bolsi A, Coray D, Emert F, Goitein G, et al. Treatment planning and verification of proton therapy using spot scanning: initial experiences. Med Phys. 2004;31(11):3150–7.
4. Lomax AJ, Boehringer T, Coray A, Egger E, Goitein G, Grossmann M, et al. Intensity-modulated proton therapy: a clinical example. Med Phys. 2000;28(3):317–24.
5. Tajima T. Prospect for compact medical laser accelerators. J Jpn Soc Therap Radiat Oncol. 1997;9(Suppl 2):83–5.
6. Malka V, Sven F, Lefebvre E, d'Humieres E, Ferrand R. Practicability of proton therapy using compact laser systems. Med Phys. 2004;31(6):1587–92.
7. Ma CM, Maughan RL. Point/counterpoint: within the next decade conventional cyclotrons for proton radiotherapy will become obsolete and replaced by far less expensive machines using compact laser systems for the acceleration of the protons. Med Phys. 2006;33(3):571–3.
8. Bulanov SV, Esirkepov T, Khoroshkov VS, Kuznetsov AV, Pegoraro F. Oncological hadrontherapy with laser ion accelerators. Phys Lett A. 2002;299:240–7.
9. Agostinelli S, Allisonas J, Amakoe K, Apostolakisa J, Araujo H, et al. Geant4–a simulation toolkit. Nucl Instrum Methods Phys Res A. 2003;506:250–303.
10. Carrier J, Archambault L, Beaulieu L, Roy R. Validation of Geant4, an object-oriented Monte Carlo toolkit, for simulations in medical physics. Med Phys. 2004;31(3):484–92.
11. Jiang H, Paganetti H. Adaptation of Geant4 to Monte Carlo dose calculations based on CT data. Med Phys. 2004;31(10):2811–8.
12. Sutherland K, Miyajima S, Date H. A simple parallelization of Geant4 on a PC cluster with static scheduling for dose calculations. First European workshop on Monte Carlo treatment planning, Journal of Physics: Conference Series. 2007; 74 012020.
13. Schneider W, Bortfeld T, Schlegel W. Correlation between CT numbers and tissue parameters needed for Monte Carlo simulations of clinical dose distributions. Phys Med Biol. 2000;45:459–78.
14. Iwase H, Niita K, Nakamura T. Development of a general-purpose particle and heavy ion transport Monte Carlo code. J Nucl Sci Technol. 2002;39(11):1142–51.
15. Niita K, Sato T, Iwase H, Nose H, Nakashima H, Sihver L. PHITS: a particle and heavy ion transport code system. Radiat Meas. 2006;41:1080–90.
16. Dendale R, et al. Proton beam radiotherapy for uveal melanoma: results of Curie Institute-Orsay Proton Therapy Center (ICPO). Int J Radiat Oncol Biol Phys. 2006;65(3):780–7.

A feasibility study of a molecular-based patient setup verification method using a parallel-plane PET system

2011 Phys. Med. Biol. 56 965

(http://iopscience.iop.org/0031-9155/56/4/006)